Liquid Crystals
Publication details, including instructions for authors and subscription information:
http://www.informaworld.com/smpp/title~content=t713926090

Synthesis and mesomorphic properties of different liquid crystal methacrylic azo monomers with 'de Vries'-like behaviour

C.M. González Henríquez[a]; E.A. Soto Bustamante[a]; D.A. Waceols Gordillo[a]; W. Haase[b]
[a] Universidad de Chile, Facultad de Ciencias Químicas y Farmacéuticas, Olivos, Santiago, Chile [b] Technische Universität Darmstadt, Institut für Physikalische Chemie, Darmstadt, Germany

Online publication date: 11 February 2010

To cite this Article González Henríquez, C.M. , Soto Bustamante, E.A. , Waceols Gordillo, D.A. and Haase, W.(2010) 'Synthesis and mesomorphic properties of different liquid crystal methacrylic azo monomers with 'de Vries'-like behaviour', Liquid Crystals, 37: 2, 217 — 225
To link to this Article: DOI: 10.1080/02678290903502007
URL: http://dx.doi.org/10.1080/02678290903502007

Liquid Crystals,
Vol. 37, No. 2, February 2010, 217–225

Taylor & Francis
Taylor & Francis Group

Synthesis and mesomorphic properties of different liquid crystal methacrylic azo monomers with 'de Vries'-like behaviour

C.M. González Henríquez[a]*, E.A. Soto Bustamante[a], D.A. Waceols Gordillo[a] and W. Haase[b]

[a]*Universidad de Chile, Facultad de Ciencias Químicas y Farmacéuticas, Olivos 1007, Santiago, Chile;* [b]*Technische Universität Darmstadt, Institut für Physikalische Chemie, Darmstadt, Germany*

(Received 18 May 2009; final version received 20 November 2009)

The synthesis and characterisation of four azo aromatic monomers, possessing two aliphatic tails, one with a methacrylate group and six methylenic units, and the other oxyhexyl or oxydodecyl, was carried out. The aliphatic tails are attached to an aromatic system consisting of two phenyl rings linked through an azo group. Two of then possess a free hydroxyl group in one of the phenyl rings. The materials were characterised by polarised light microscopy, differential thermal analysis and X-ray diffraction. In the cooling cycle, M6OA8 exhibits a smectic A (SmA) phase throughout the liquid crystalline range, whereas M6A12 develops SmA and SmC mesophases; other monomers show a phase transition from SmA to a 'de Vries'-like phase. The photoisomerisation of the chromophores was studied in solution by irradiation at different wavelengths.

Keywords: azo aromatic monomers; de Vries phase; photoisomerisation

1. Introduction

In the last decade [1] the studies of liquid crystals (LCs) for display application have been increased, due to their low voltage and good compatibility as integrated circuit (IC) drivers. Liquid crystal displays (LCDs) are used in watches, electronic calculators, television, notebooks and so on. For such applications the alignment of the LC layer is extremely important and usually polyimides [2], which are amorphous polymers with a high molecular weight, are used. These materials produce thermal stability in the system, due to the anchoring of the molecules in the polymeric network. An alternative to achieving the alignment is the use of materials that present photoisomerisation influenced by light at a specific wavelength [3–16]. In 1983 to 1984, Todorov *et al.* reported that azo compounds could be used for holographic storage and photonic device applications [17,18], in a so-called photoalignment process.

A peculiar phenomenon has been observed in chiral smectic LCs, where the molecules tilt but the layers do not contract [19]. Usually this phenomenon has been seen as a function of decreasing temperature into the smectic-C* phase or under an applied electric field in the smectic-A (SmA) phase. Adrien de Vries and colleagues have suggested that it is caused by a disordered molecular orientation in the SmA phase, which becomes more ordered under decreasing temperature or increasing electric field [20–22]. LCs exhibiting this behaviour are generally called de Vries materials [23].

In this work we attempt to develop materials that later on can be used to obtain polymeric networks that can be photoaligned. The acronym M6(*R*)A*n* used is in accordance with our previous work [24–26], where a methacrylate group with six methylene units as spacer (M6) is bonded to the aromatic group, consisting of two phenyl rings linked through an azo linkage (A). In the aromatic core, one of the phenyl rings remains with (OA) or without (A) a hydroxyl group in the *meta* position. The aromatic group possesses, in its *para* position, an alkoxy flying tail with *n* methylene units (8 and 12). The general structure of the monomers is shown in Figure 1.

The four monomers were prepared, and their liquid crystalline phases as well as the $E \rightarrow Z$ photoisomerisation process in solution characterised. We found that the modification in the aromatic core of the molecule or the variation of the number of methylene units used as the ealkoxy flying tail led to different mesophase sequences. Longer monomers with dodecloxy alkyl chains show enantiotropic SmA–smectic-C (SmC) second-order phase transitions. Shorter monomers with octyloxy alkyl chains show first-order phase transitions and in the case of M6OA8 no SmC phase was observed. No isomerisation process in the hydroxyl-containing monomers M6OA8 and M6OA12 was established. The other compounds photoisomerise at time frames comparable with those in the literature. Studies of *E–Z* isomerisation in thin films coated over a glass surface show an interesting photoalignment process that will be reported elsewhere.

*Corresponding author. Email: carmengh@ciq.uchile.cl

ISSN 0267-8292 print/ISSN 1366-5855 online

DOI: 10.1080/02678290903502007
http://www.informaworld.com

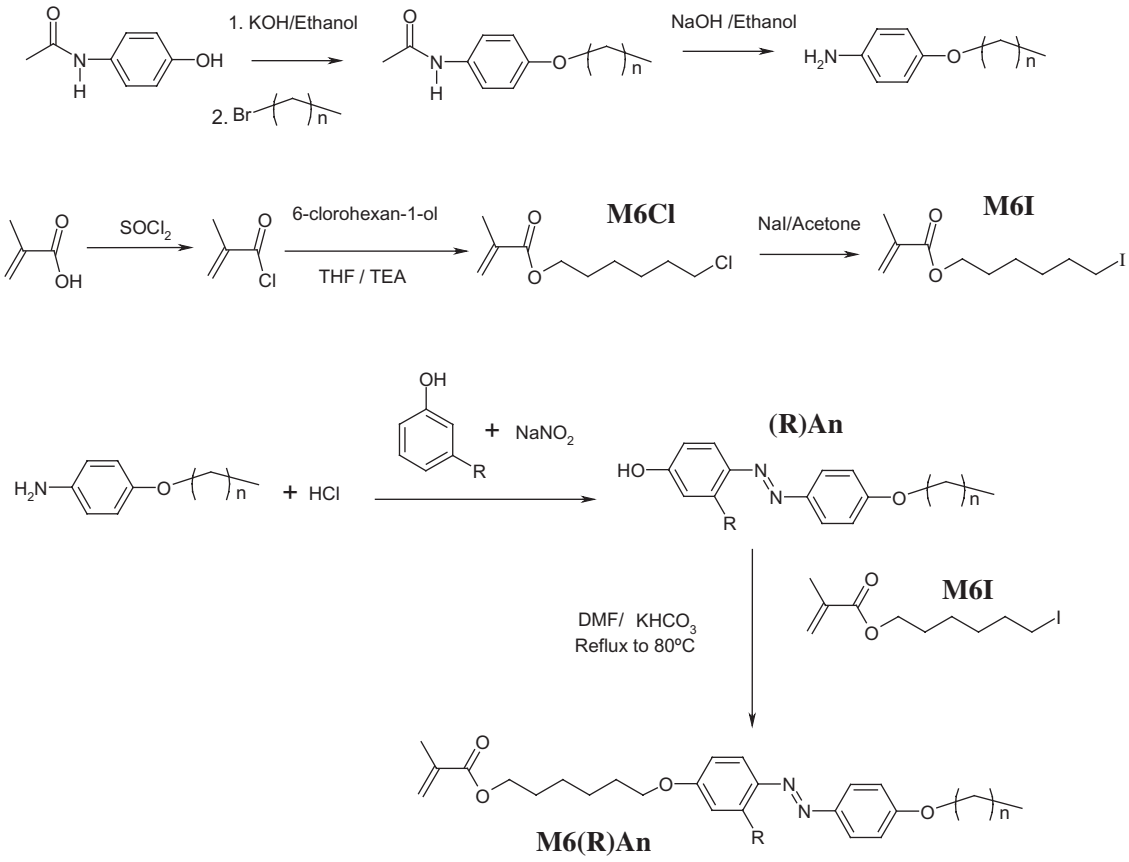

Figure 1. Synthetic route for the preparation of the azo monomers: M6A12 ($R = H$, $n = 12$); M6A8 ($R = H$, $n = 8$); M6OA12 ($R = OH$, $n = 12$) and M6OA8 ($R = OH$, $n = 8$).

2. Experimental conditions

The syntheses of all azo aromatic monomers were carried out using a convergent synthetic pathway. The compounds investigated were characterised by ^{1}H-NMR (nuclear magnetic resonance) spectroscopy (300 MHz spectrometer Bruker, WM 300) and elemental analysis (Perkin Elmer, 240B). The final compounds were also characterised by ^{13}C-NMR, using the same spectrometer and by high-resolution mass spectrometry (HRMS, Thermo Finnigan model MAT 95 XI mass spectrometer).

A polarising microscope (Leica, DLMP), equipped with a heating stage (HS-1, Instec) was used for temperature-dependent investigations of LC textures. A video camera (Panasonic, WVCP414P), installed on the polarising microscope, was coupled with a video capture card (Miro DC-30), allowing real time capture and image saving. The samples were supported between glass plates or suspended in a copper plate with a 2 mm diameter hole. A differential thermal analyser (DTA) (Mettler, FP90 DTA) with indium as calibration standard was used to investigate the thermal behaviour, using heating and cooling rate of 10°C/min. This technique is similar to differential scanning calorimetry because it gives the enthalpy values by comparison with different standards at different temperatures.

Small-angle X-ray measurements were carried out using a horizontal two-circle X-ray diffractometer STOE STADI 2 (Cu Kα radiation) (Stoe GmbH) with a linear position-sensitive detector for data collection; the aligned samples were contained in 0.8mm glass capillaries (Lindemann) and held in a copper block. The temperature was stabilised in the range 30–100°C at ±0.1 K during the measurements. The samples were oriented using permanent magnets with a field strength of 0.3 T.

The ultraviolet (UV)–visible (Vis) spectra in tetrahydrofurane (THF) solution were recorded in an ATI Unicam UV–Vis Spectrometer UV3. The light source for photoirradiation was a 450 W medium pressure mercury lamp (Model B 100 AP) for $E \rightarrow Z$ acting at 360 nm, and a commercial dichroic lamp of 50 W for $Z \rightarrow E$ isomerisation to reach 450 nm. In the case of the mercury lamp, a bandwidth filter with two specific wavelengths at 366 nm and 746 nm (50.27% and

9.47% transmittance) was used. In the case of the dichroic lamp, a Vis filter with a cut-off at 392 nm (80–89% transmittance) was employed to avoid any radiation coming from 360 nm.

3. Experimental section

3.1 Preparation of azoaromatic monomers

The monomers were prepared by coupling the corresponding aniline with the phenolic compound and finally etherification was carried out with the previously prepared methacrylic iodide, following the method described in [24]. The synthesis of the aniline is described in detail in [27]. The total synthetic route is shown in Figure 1. Following this scheme, four aromatic monomers containing azo groups were synthesised, two of them using resorcinol and the other two using phenol.

3.1.1 4-{[4-(dodecyloxy)-phenyl)-diazenyl}-phenol (A12) ($C_{24}H_{34}O_2N_2$)

The 4-(dodecyloxy) aniline (5.54 g, 0.02 mol) was dissolved in an ethanol/acetonitrile mixture cooled in an ice bath, and a cold solution of HCl (0.2 mol) was added dropwise to keep the temperature below 5°C. Afterwards, a previously prepared solution of phenol (2 g, 0.02 mol), sodium nitrite (1.6 g, 0.023 mmol) and potassium hydroxide (1.12 g, 0.02 mol), dissolved in the same solvent, was added. The reaction mixture was stirred for 2 hours, keeping the temperature at –5°C. The product was collected from the reaction mixture as a brown-red solid after neutralisation of the reaction mixture with diluted HCl. The solid product was recrystallised in dichloromethane. The total yield for A12 and A8 was 59%.

^{1}H-NMR ($CDCl_3$) δ ppm: 7.80 (AA'd, 2H, N=N–Har–OC8), 7.78 (AA'd, 2H, OH–ArH–N=N–), 6.92 (BB'd, 2H, N=N–ArH–OC8), 6.84 (BB'd, 2H, HO–Har–N=N–), 5.55 (br.s, OH–Ar–), 3.96 (t, 2H, –O–CH_2–), 1.76 (m, 2H, –O–βCH_2–), 1.52 (m, 2H, –O–γCH_2–), 1.40–1.22 (m, 16H –CH_2–), 0.82 (t, 3H, –CH_3–).

3.1.2 4-{[4- (octyloxy)-phenyl)diazenyl}-phenol (A8) ($C_{20}H_{26}O_2N_2$)

^{1}H-NMR ($CDCl_3$) δ ppm: 7.79 (AA'd, 2H, N=N–HAr–OC8), 7.76 (AA'd, 2H, OH–ArH–N=N–), 6.91 (BB'd, 2H, N=N–ArH–OC8), 6.86 (BB'd, 2H, HO–HAr–N=N–), 5.57 (br.s, OH–Ar–), 3.98 (t, 2H, –O–CH_2–), 1.77 (m, 2H, –O–βCH_2–), 1.53 (m, 2H, –O–γCH_2–), 1.40–1.22 (m, 8H, –CH_2–),0.82 (t, 3H, –CH_3–).

3.1.3 5-(dodecyloxy)-2-[(4-hydroxyphenyl)-diazenyl] -phenol (OA12) ($C_{24}H_{34}O_3N_2$)

The same procedure as for A12 was carried out, replacing the phenol with resorcinol. The crude product of orange colour was purified by column chromatography over silica gel, using hexane/ ethyl acetate 4:1 as eluent.

^{1}H-NMR ($CDCl_3$) δ ppm: 7.69 (AA'd, 2H, N=N–HAr), 7.65 (d, 1H, HO–ArH_6), 6.91 (BB'd, 2H, N=N–ArH–O–), 6.45 (dd, 1H, HO–ArH_5–), 6.35 (d, 1H, HO–ArH_3–), 5.5 (br.s, OH–Ar–), 3.95 (t, 2H, –O–CH_2–), 1.79 (m, 2H, –O–βCH_2–), 1.51 (m, 2H, –O–γCH_2–), 1.40–1.19 (m, 16H, –CH_2–),0.81 (t, 3H, –CH_3–).Yield: 55%.

3.1.4 5-(octyloxy)-2-[(4-hydroxyphenil)-diazenyl]-phenol (OA8) ($C_{20}H_{26}O_3N_2$)

^{1}H-NMR ($CDCl_3$) δ ppm: 7.71 (AA'd, 2H, N=N–HAr), 7.63 (d, 1H, HO–ArH_6), 6.92 (BB'd, 2H, N=N–ArH–O–), 6.47 (dd, 1H, HO–ArH_5–), 6.35 (d, 1H, HO–ArH_3–), 5.44 (br.s, OH–Ar–), 3.95 (t, 2H, –O–CH_2–), 1.78 (m, 2H, –O–βCH_2–), 1.51 (m, 2H, –O–γCH_2–), 1.40–1.25 (m, 8H, –CH_2–),0.82 (t, 3H, –CH_3–). Yield: 55%.

3.1.5 Alkylation of the azo compounds

The precursor 4-{[4-(octyloxy)-phenyl)-diazenyl}-phenol (A8) was dissolved in dimethylformamide and mixed with $KHCO_3$ (0.6 g, 0.0061 mol) and a small amount of hydroquinone. The solution was heated at 80°C for 1 hour. After this time, the compound M6I (1.8 g, 0.0061 mol) was added to the reaction mixture under continuous heating for another 24 hours. After heating, the product was extracted twice with diethyl ether, and then the combined ether extracts were washed with water to eliminate the solvent (DMF). Subsequently, the solution was dried over anhydrous $MgSO_4$. The solvent was evaporated and the crude product purified by column chromatography over silica gel using hexane and ethyl acetate as the eluent (relation 4:1). The total yield of the reaction for compound M6A8 was 46.1% and 44.7% for compound M6A12.

[{4-[(E)-(4-octyloxyphenyl)diazenyl]phenoxy}hexyl]-2-methylprop-2-enoate, M6A8 ($C_{30}H_{43}O_4N_2$)

^{1}H-NMR ($CDCl_3$) δ ppm: 7.89 (AA'd, 2H, N=N–HAr–OC8), 7.86 (AA'd, 2H, OH–ArH–N=N–), 6.94 (BB'd, 2H, N=N–ArH–OC8), 6.91 (BB'd, 2H, HO–HAr–N=N–), 6.02 (ps.s, 1H, *Trans* H_2C=C), 5.47 (ps.s, 1H, *Cis* H_2C=C), 4.02 (t, 2H, –O–CH_2–), 3.78 (m,

2H, –Ar–O–CH_2–), 3.96 (m, 2H,CO_2–CH_2–), 1.94 (ps.s, 3H, CH_3–CO), 1.79 (m, 2H, –O–βCH_2–), 1.43–1.25 (m, 18H, –CH_2–), 0.80 (t, 3H, –CH_3–).

Elemental analysis: theoretical C: 71.54, H: 8.93, N: 5.23; experimental C: 72.84, H: 8.56, N: 5.66.

[{4-[(E)-(4-dodecyloxyphenyl)diazenyl]phenoxy} hexyl]-2-methylprop-2-enoate, M6A12 ($C_{34}H_{51}O_4N_2$)

^{1}H-NMR ($CDCl_3$) δ ppm: 7.86 (AA'd, 2H, N=N–HAr–OC8), 7.82 (AA'd, 2H, OH–ArH–N=N–), 6.94 (BB'd, 2H, N=N–ArH–OC8), 6.81 (BB'd, 2H, HO–HAr–N=N–), 6.03 (ps.s, 1H, *Trans* H_2C=C), 5.49 (ps.s, 1H, *Cis* H_2C=C), 4.10 (t, 2H, –O–CH_2–), 3.97 (m, 4H,CH_2–O–Ar–N=N–Ar–O–CH_2–), 1.87 (ps.s, 3H, CH_3–CO), 1.75–1.20 (m, 28H, –CH_2–), 0.81 (t, 3H, –CH_3–).

^{13}C-NMR ($CDCl_3$) δ ppm: 167.473 (1C, CH_3–$C(CH_2)$–C(O)=O); 161.133 (2C, –C(Ar)–); 146.930 (4C, –C(Ar)–); 136.443 (1C, CH_3–$C(CH_2)$–C=O); 125.191 (1C, CH_2=$CH(CH_3)$); 124.246 (2C,–C(Ar)–); 114.604 (4C, –C(Ar)–); 77.409 (2C, Ar–O–CH_2–); 68.280 (1C, –C–O–CH_2–), 31.882–25.704 (13C, –CH_2–); 22.653 (1C, –CH_2–CH_3); 18.295 (1C, CH_3–$C(CH_2)$–C=O); 14.086 (1C, –CH_3).

HRMS (electron ionisation (EI), 70 eV). Calculated for $C_{34}H_{51}O_4N_2$ (M+): 550.37708, found: 550.3750.

Elemental analysis: theoretical C: 73.39, H: 9.40, N: 5.35; experimental C: 74.14, H: 9.15, N: 5.09.

[{3-hydroxy-4-[(E)-(4-octyloxyphenyl)diazenyl] phenoxy}hexyl]-2-methylprop-2-enoate, M6OA8 ($C_{30}H_{43}O_5N_2$)

^{1}H-NMR ($CDCl_3$) δ ppm: 13.61 (s, 1H, OH–Ar–), 7.73 (AA'd, 2H, N=N–HAr), 7.64 (d, 1H, O–ArH_6), 6.90 (BB'd, 2H, N=N–ArH–O–), 6.51 (dd, 1H, HO–Ar(OH)H_5–), 6.46 (d, 1H, O–ArH_3–), 6.03 (ps.s, 1H, *Trans* H_2C=C), 5.48 (ps.s, 1H, *Cis* H_2C=C), 4.09 (t, 2H, –O–CH_2–), 3.95 (m, 4H, –Ar–O–CH_2), 2.09 (m, 3H, CH_3–CO), 1.88–1.23 (m, 20H, –CH_2–), 0.82 (t, 3H, –CH_3–).

Elemental analysis: theoretical C: 70.53, H: 8.79, N: 5.23; experimental C: 70.56, H: 8.29, N: 5.49.

[{3-hydroxy-4-[(E)-(4-dodecyloxyphenyl)diazenyl] phenoxy}hexyl]-2-methylprop-2-enoate, M6OA12 ($C_{34}H_{51}O_5N_2$)

^{1}H-NMR ($CDCl_3$) δ ppm: 13.60 (s, 1H, OH–Ar–), 7.71 (AA'd, 2H, N=N–HAr), 7.67 (d, 1H, HO–ArH_6), 6.90 (BB'd, 2H, N=N–ArH–O–), 6.53 (dd, 1H, HO–ArH_5–), 6.47 (d, 1H, HO–ArH_3–), 6.03 (ps.s, 1H, *Trans* H_2C=C), 5.48 (ps.s, 1H, *Cis* H_2C=C), 4.09 (t, 2H, –O–CH_2–), 3.96–3.94 (m, 4H, CO_2–CH_2– and –CH_2–O–Ar–), 2.09 (m, 3H, CH_3–CO), 1.88–1.25 (m, 28H, –CH_2–),0.82 (t, 3H, CH_3–).

^{13}C-NMR ($CDCl_3$) δ ppm: 167.522 (1C, CH_3–$C(CH_2)$–C(O)=O); 162.611 (1C, –C(Ar)–); 161.046 (1C, Ar(C)–O–); 144.234 (1C, Ar(C–OH); 136.479 (1C, CH_3–$C(CH_2)$–C=O); 133.995 (3C, –Ar(C)–); 125.238 (1C, CH_2=$CH(CH_3)$); 123.292 (1C, –C(Ar)–); 114.966 (2C, –C(Ar)–); 108.124 (2C, Ar(C)–N=N–(Ar(C)–); 101.887 (1C, –C(Ar)–); 76.586 (2C, Ar–O–CH_2–); 68.394 (1C, –C–O–CH_2–), 31.914–25.714 (13C, –CH_2–); 22.687 (1C, –CH_2–CH_3); 18.333 (1C, CH_3–$C(CH_2)$–C=O); 14.118 (1C, –CH_3).

HRMS (EI, 70 eV). Calculated for $C_{34}H_{51}O_5N_2$ (M+): 566.37195, found: 566.3704.

Elemental analysis: theoretical C: 71.20, H: 9.20, N: 5.16; experimental C: 72.05, H: 8.89, N: 4.94.

4. Results and discussion

4.1 Synthesis

Polymerisable monomers not bearing a hydroxyl group of similar structure have been described in the literature [28]. The identification of each one of the products shown in the synthetic route was verified with ^{1}H-NMR. The difference between monomeric structures with and without a hydroxyl group in the aromatic core is easy to distinguish by inspecting the protons in the aromatic core and detecting the presence of the hydroxyl group at low field. To differentiate between shorter and longer monomers, it is just necessary to quantify the proton signals at high field in the spectra that belong to the aliphatic chains.

4.2 Texture identifications

The textures obtained using polarised light microscopy, as shown in Figures 2(a) and (b), give a perfect system of Dupin cyclides characteristic of the focal conic SmA phase. This topology consists of smectic layers which are arranged basically perpendicular to the substrate of the plane by producing an ellipse. These textures are obtained below the transition to the isotropic state. Figures 2(c) and (d) show the SmC phase, where all singularities possess four brushes with $s = \pm 1$; this texture is called Schlieren and the brushes appear smoother and somewhat washed out for the SmC phase.

4.3 Thermodynamic results

Table 1 summarises the phase transition temperatures for all compounds. These data are obtained from DTA experiments using 5°C/min as cooling and heating rates. The phase transition temperatures for the

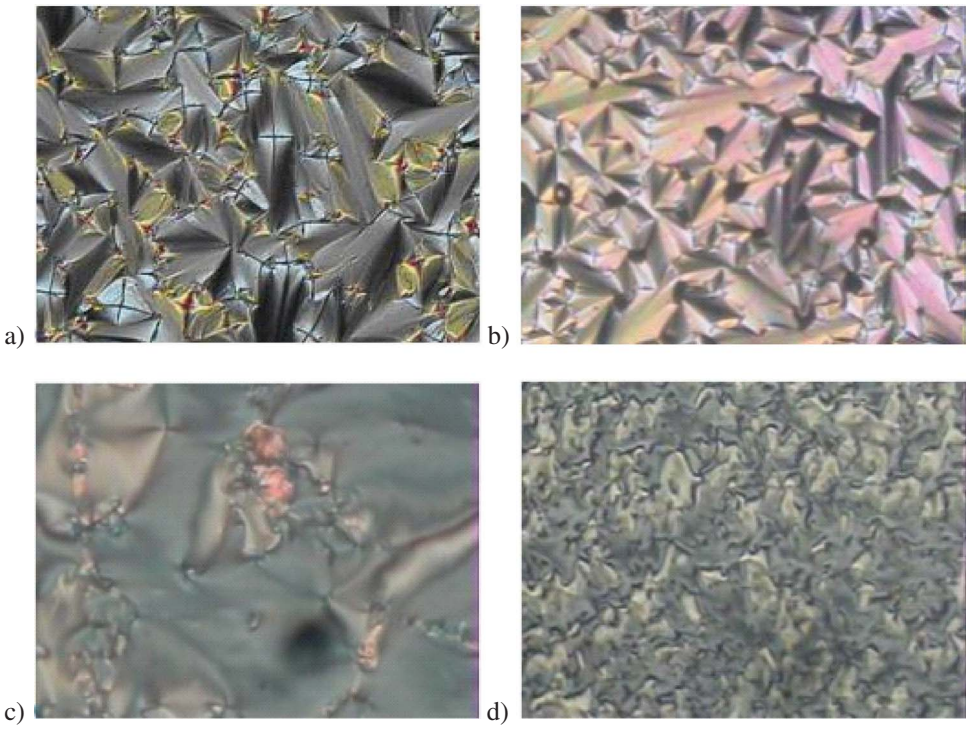

Figure 2. Observed textures: (a) SmA (M6A12, $T = 82°C$); (b) SmA (M6A8, $T = 80°C$); (c) SmC (M6OA12, $T = 60°C$) and (d) SmC (M6A12, $T = 67°C$).

Table 1. Phase transition temperatures and enthalpy for the azo monomers under investigation.

Compounds	Heating	Cooling
M6A8	C1–66.1°C (8.9 J g^{-1})–C2–75.5°C (59.3 J g^{-1}) – SmC–83.6°C(3.3 J g^{-1})–SmA–89.1°C (3.5 J g^{-1})–I	I–87.1°C (–3.9 J g^{-1})–SmA–81.4°C (–3.1 J g^{-1})–SmC–55.8°C (–74.7 J g^{-1})–C2–45.2°C (–1.40 J g^{-1})–C1
M6A12	C–76.1°C (81.9 J g^{-1})–SmC–84.0°C* SmA– 90.1°C (12.8 J g^{-1})–I	I–86.8°C (–14.5 J g^{-1})–SmA–79.5°C*–SmC–52.8°C (–50.3 J g^{-1})–C
M6OA12	C1–28.7°C (15.5 J g^{-1})–C2–35.4°C (24.7 J g^{-1})– SmC–74.6°C–SmA–98.0°C (21.8 J g^{-1})–I	I–94.4°C (–23.4 J g^{-1})–SmA–71.3°C*–SmC–23.6°C (–16.3 J g^{-1})–C
M6OA8	C–45.4°C (67.2 J g^{-1})–SmA–89.3°C (11.8 J g^{-1})–I	I–85.1°C(–9.4 J g^{-1})–SmA–n.d.–C(<26.8°C)

*Observed for PLM; n.d. = not determined for DTA.

monomers were taken from the onset of the maximum temperature in the DTA enthalpic peaks.

For the transition from the SmA phase to the SmC phase, the situation is different considering the structure of the monomers. In the case of M6A8 these enthalpy values correspond to a first-order transition, whereas for M6OA12 a second-order transition is present which is just detectable by polarised light microscopy (PLM). Compounds M6A12 and M6OA8 only possess a SmC and SmA phase, respectively.

4.4 X-ray studies

X-ray studies were carried out for all four representative compounds: M6A12, M6A8, M6OA12 and M6OA8. The X-ray data below the transition point to the isotropic state showed sharp small-angle peaks reflecting a smectic character for all mesophases and diffuse wide-angle halos (see Figure 3(a)) related to the degree of disorder within the smectic layers. The experimental interlayer spacings (d), taken from X-ray measurements, are displayed in Figure 3(b).

The broad peaks in the wide-angle region permit us to calculate the average intermolecular distances D within the smectic layers. These peaks were fitted by Lorentzian line shapes (solid lines); giving values between 15° and 25° in 2θ (see Figure 3(a)). Thus molecular packing within the smectic layers must be considered to be liquid-like. When the temperature increases a d-value dependence attributed to the SmC

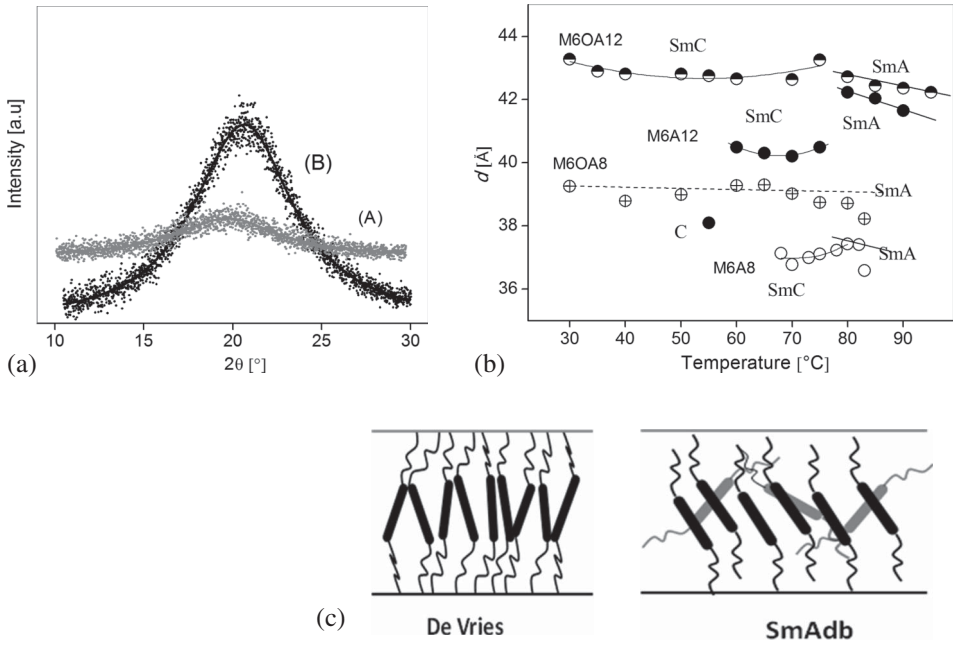

Figure 3. (a) Diffuse wide angle halos, showing liquid-like in-plane order: M6OA12 (A) 95°C; (B) 60°C. The solid lines correspond to the Lorentzian fit of the data. (b) Temperature dependence of the interlayer distance by cooling. (c) De Vries and SmA_{db} models.

to SmA phase transitions can be distinguished for the M6A12, M6OA12 and M6A8 compounds. On the other hand, the M6OA8 monomer showed only a monotonic behaviour of the interlayer distance with temperature, which is characteristic of the SmA phase. These data are in accordance with the results obtained from PLM analysis. The interlayer distances are greater for the compounds that have an alkoxy flying tails with 12 methylene units, due to the presence of an additional four methylenic groups than in the oxyoctyl derivatives. When comparing molecules with and without a hydroxyl group, that is M6OA8 and M6OA12 with M6A8 and M6A12 respectively, the former also show larger interlayer distances.

Interestingly, all compounds show a larger interlayer distance compared to their corresponding molecular length L. The value of L was calculated using Hartree Fock (HF) and post Hartree Fock calculation such as MP2 methods (GAMESS program package) [29] with the 631G* basis sets. Then, the molecular length L arounds 33.69 Å and 38.76 Å for M6A8/M6OA8 and M6A12/M6OA12, respectively. On the other hand, the experimental value of d is 36 Å/39 Å and 40 Å/44 Å for each couple. This behaviour must be attributed to the existence of an interdigitated smectic phase, most probably a SmA_d phase, with layer spacing 1.2 to 1.3 times the molecular length, where the aliphatic chains from one layer formed from dimers are interdigitated with those of neighbouring layers.

Going further by cooling, a more peculiar situation is observed, with a layer period incommensurate with the length of the individual molecules [30, 31]. The layer spacing, derived from X-ray diffraction profiles, obtained as a function of temperature in the smectic region (see Figure 3(b)), does not decrease with temperature as it usually does in the SmC phase. This phenomenon is clearly seen for compounds M6OA12 and M6A8, and is less evident for M6A12. Two reasons can be argued for this behaviour:

(1) De Vries behaviour: Smectic LCs form layers with a thickness of one molecular length. Therefore, when the molecules tilt in the SmC phase, one would expect layer shrinking as occurs in most cases. The de Vries SmA phase is different: although the optical axis is normal to the layers, an average molecular tilt respective to the layer normal is found [32].
(2) Biaxial SmA: Pratibha *et al.* [33] reported a SmA_{db} phase in molecules with a highly polar cyano group at one terminal position which overlaps in an antiparallel orientation. They describe the phenomenon as a direct transition from the uniaxial SmA_d phase to a biaxial SmA (SmA_{db}, see Figure 3(c)) phase on a lowering of the temperature, exactly as we observed for three of our compounds. Recently, they described the same phase in non-symmetric LC dimers comprising two rod-like anisometric segments [34].

We believe that in our case the presence of a SmA_{db} phase cannot be responsible for the incommensurate SmA phase, with longer interlayer distance. The prepared monomers do not possess strong polar groups, which are required for the existence of the phase. On the other hand, in the monomers with 'de Vries'-like phase, the smectic layer spacing slightly decreases within the phase (see Figure 3(b)), resulting in a negligible shrinkage of the SmA_d phase. The practical absence of layer shrinkage clearly confirms the 'de Vries' character of the mesophase, where the tilt develops without substantial changes in the smectic layer thickness (Figure 3(c)).

4.5 *Photoresponsive properties*

The occurrence of *E*–*Z* photoisomerisation of the M6A12 monomer was investigated in solution. Figure 4 shows the UV–Vis spectra of LC azo monomer dissolved in THF. After 30 s under UV light irradiation, the high-intensity absorption peak of azobenzene in the *E* form centred at 359 nm (π–π^* transition) almost disappears, and is replaced by a low-intensity absorption peak of azobenzene in the *Z* conformation near 450 nm (n–π^*). The UV irradiation caused both the diminution in absorbance around 359 nm and an increase in the absorbance at 450 nm, indicating the $E \rightarrow Z$ photoisomerisation.

As the *E* isomer is more stable than the *Z* isomer, the molecule in the *Z* form may relax back to the *E* form by one of two mechanisms: (1) a spontaneous thermal backreaction or (2) a reverse $Z \rightarrow E$ photoisomerisation cycle. As the complete $Z \rightarrow E$ thermal backreaction generally requires several hours at room temperature, the *Z* isomer can be considered as stable on a time scale of minutes.

Then, visible light at 450 nm induced $Z \rightarrow E$ photoisomerisation of the azobenzene. The quantity of molecules that relax back through this process is slightly less (see Figure 4(b)) than the amount of molecules that initially transit from the $E \rightarrow Z$ conformation due to UV light exposure (see Figure 4(a)). Next, if a subsequent visible light irradiation of 450 nm is applied with a cut-off filter at 450 nm, the absorption peak of *E* azobenzene is recovered as a result of the $Z \rightarrow E$ back isomerisation. In the dark, the thermal relaxation of *Z* azobenzene takes place slowly, needing hours to complete. An additional experiment was carried out, leaving the compound that was irradiated for 1 hour, and already in the *E* conformation, for 12 hours in darkness without irradiation. No changes in the UV–Vis spectra were detected.

The monomers with OH group were also investigated, but no changes in the UV–Vis spectra were observed. We modified Figure 4(a) to include the spectra of M6OA12 to clarify this point.

The ratio of the *E* and *Z* forms of the azo compounds produced for the UV and Vis irradiation was determined by means of Equations (1) [35] and (2). To estimate the percentage of *Z* azobenzene in the photostationary state, Equation (1) was used. Here, A_0 and A_z correspond to the absorbance at 359 nm before irradiation and at any time during irradiation, respectively. When the conversion reaches about 100%, we can estimate the irradiation time for the full $E \rightarrow Z$ isomerisation:

$$\%Z = 100(A_0 - A_Z)/A_0. \quad (1)$$

The percentage of *E* azobenzene in the photostationary state was determined by means of Equation (2), where A_0 and A_E are the absorbance at 359 nm before irradiation and at any time during irradiation with 450 nm wavelength, respectively:

$$\%E = 100(A_E)/A_0. \quad (2)$$

Figure 5 summarises the results obtained using this formula and the corresponding absorptions at

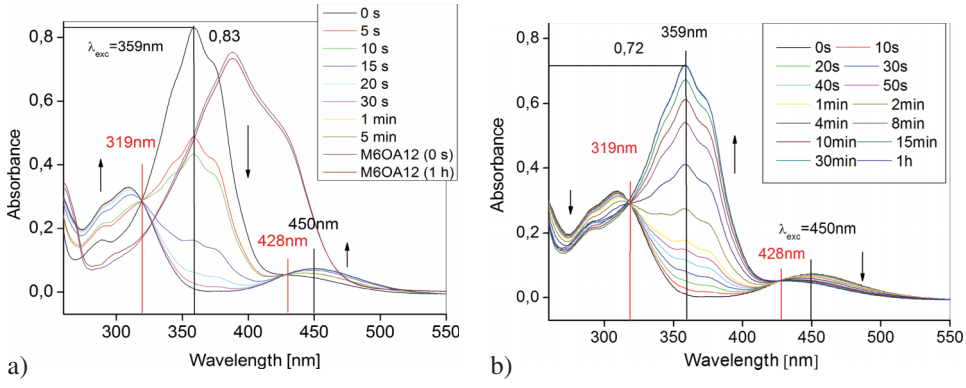

Figure 4. Changes in the absorption spectra for the M6A12 monomer: (a) $E \rightarrow Z$ and (b) $Z \rightarrow E$ photoisomerisation.

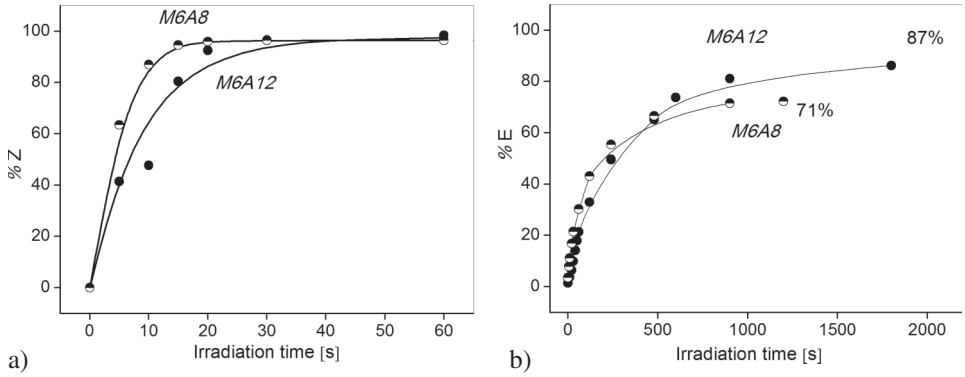

Figure 5. Irradiation time for azobenzene compounds: conversion rate of (a) %*Z* and (b) %*E*.

various times taken from the experiments carried out in the THF solutions. Within the first few seconds a very fast change in the chromophores is observed (see Figure 5(a)), with a transition to the *Z* configuration taking place, reaching a maximum with 96–98% conversion. In contrast, the reverse isomerisation is rather slow, perhaps due to the lower intensity of the visible lamp compared with the UV–Vis one (Figure 5(b)).

5. Conclusions

The synthesis of new azo aromatic monomers has been carried out. All compounds exhibited a thermotropic liquid crystalline behaviour, characterised by PLM, DTA and X-Ray diffractometry.

Lateral substitution affects the occurrence of the SmC phase in the case of shorter monomers probably due to strong hydrogen bonding interactions in the orthogonal SmA phase. Also the increase in the aliphatic chain produces a smooth transition from the SmA to the 'de Vries'-like phase by cooling, which is reflected in the second-order phase transition observed. This behaviour can be explained by the increase in the molecular flexibility.

Monomers without hydroxyl group are capable of photoisomerisation using the usual irradiation wavelengths of 366 and 450 nm. The isomerisation process takes place at time frames comparable with those in the literature [4], that is, between 30 seconds for the $E \rightarrow Z$ process and 1 minute for the reverse $Z \rightarrow E$ process.

Acknowledgements

C.M. González-Henríquez acknowledges a Scholarship from Conicyt and E.A. Soto-Bustamante is grateful for financial support from Project FONDECYT 2007 Nr. 1071059 and Merck Chile S.A.

References

[1] Otón, J.M.; Quintana, X.; Castillo, P.I.; Lara, A.; Urruchi, V.; Bennis, N. *Opto-Electron. Rev.* **2004**, *12*, 263–269.
[2] Geary, J.M.; Goodby, J.W.; Kmetz, A.R.; Patel, S. *J. Appl. Phys.* **1987**, *62*, 4100–4108.
[3] Zhao, Y. *Pure Appl. Chem.* **2004**, *76*, 1499–1508.
[4] Wang, G.; Leclair, S.; Roy, L.; Moltallebi, S.; Zhao, Y. *Liq. Cryst*. **2005**, *32*, 125–131.
[5] Natansohn, A.; Rochon, P. *Chem. Rev.* **2002**, *102*, 4139–4176.
[6] Ichimura, K. *Chem Rev.* **2000**, *100*, 1847–1874.
[7] Rochon, P.; Gosselin, J.; Natansohn, A.; Xie, S. *Appl. Phys. Lett.* **1992**, *60*, 4–5.
[8] Geue, Th.; Ziegeler, A.; Stumpe, J. *Macromolecules* **1997**, *30*, 5279–5284.
[9] Rochon, P.; Batalla, E.; Natansohn, A. *Appl. Phys. Lett*. **1995**, *66*, 136–138.
[10] Song, O.K.; Wang, C.H.; Pauley, M.A. *Macromolecules* **1997**, *30*, 6913–6919.
[11] Wu, Y.; Demachi, Y.; Tsutsumi, O.; Kanazawa, A; Shiono. T.; Ikeda, T. *Macromolecules* **1998**, *31*, 349–354.
[12] Natansohn, A.; Rochon, P.; Gosselin, J.; Xie, S. *Macromolecules* **1992**, *25*, 2268–2273.
[13] Rasmussen, P.H.; Ranamujam, P.S.; Hvilsted, S.; Berg, R.H. *J. Am. Chem. Soc.* **1999**, *121*, 4738–4743.
[14] Bai, S.; Zao, Y. *Macromolecules* **2002**, *35*, 9657–9664.
[15] Leclair, S.; Mathew, L.; Giguere, M.; Motallebi, S.; Zhao, Y. *Macromolecules* **2003**, *36*, 9024–9032.
[16] Sévigny, S.; Bouchard, L.; Motallebi, S.; Zhao, Y. *Macromolecules* **2003**, *36*, 9033–9041.
[17] Todorov, T.; Nikolova, L.; Tomova, N. *Appl. Opt.* **1984**, *23*, 4309–4312
[18] Todorov, T.; Nikolova, L.; Stoyanova, K.; Tomova, N. *Appl. Opt.* **1985**, *24*, 785–788.
[19] Ratna, B.R.; Shashidhar, R.; Nair G.G.; Prasad, S.K.; Bahr, C.; Heppke, G. *Phys. Rev. A: At., Mol., Opt. Phys.* **1988**, *37*, 1824–1826.
[20] de Vries, A. *Mol. Cryst. Liq. Cryst*. **1977**, *41*, 27–31.
[21] de Vries, A.; Ekachai, A.; Spielberg, N. *Mol. Cryst. Liq. Cryst.* **1979**, *49*, 143–152.
[22] de Vries, A. *Mol. Cryst. Liq. Cryst.* **1979**, *49*, 179–185.
[23] Hayashi, N.; Kato, T.; Fukuda, A.; Vij, J.K.; Panarin, Y.P.; Naciri, J.; Shashidhar, R.; Kawada, S.; Kondoh, S. *Phys. Rev. E: Stat., Nonlinear, Soft Matter Phys.* **2005**, *71*, 041705–041712.

[24] Soto Bustamante, E.A.; Yablonsky, S.V.; Beresnev, L.A.; Blinov, L.M.; Haase, W.; Dultz, W.; Galyametdinov, Yu.G. Methode zur Herstellung von polymeren pyroelektrischen und piezoelektrischen Elementen, German Patent No. 195 47 934.3, 20 Dic 1995, DE 195 47 934 A1, 26 June 1997, European Patent EP 0 780 914 A1 25 June 1997, Japanese Patent JP 237921/907 09 September 1997, US Patent US 5 833 833, 10 November 1998.
[25] Soto Bustamante, E.A.; Yablonsky, S.V.; Ostrovskii, B.I.; Beresnev, L.A.; Blinov, L.M.; Haase, W. *Chem. Phys. Lett.* **1996**, *260*, 447–452.
[26] Soto-Bustamante, E.A.; Saldaño-Hurtado, D.; Vergara-Toloza, R.O.; Navarrete-Encina, P.A. *Liq. Cryst.* **2000**, *30*, 17–22
[27] Soto Bustamante, E.A.; Haase, W. *Liq. Cryst.* **1997**, *23*, 603–612.
[28] Bai, S.; Zhao, Y. *Macromolecules* **2002**, *35*, 9657–9664.
[29] Schmidt, M.W.; Baldridge, K.K.; Boatz, J.A.; Elbert, S.T.; Gordon, M.S.; Jensen, J.H.; Koseki, S.; Matsunaga, N.; Nguyen, K.A.; Su, S.; Windus, T.L.; Dupuis, M.; Montgomery J.A. *J. Comput. Chem*. **1993**, *14*, 1347–1363.
[30] Levelut, A.M.; Tarento, R.J. *Phys. Rev. A: At., Mol., Opt. Phys.* **1981**, *24*, 2180–2186.
[31] Ostrovskii, B.I. *Soviet Sci. Rev. A* **12**, *2*, 85–146.
[32] Rössle, M.; Braun, L.; Schollmeyer, D.; Zentel, R.; Lagerwall, J.P.F.; Giesselmann, F.; Stannarius, R. *Liq. Cryst.* **2005**, *32*, 533–538.
[33] Pratibha, R.; Madhusudana, N.V.; Sadashiva, B.K. *Phys. Rev. E: Stat., Nonlinear, Soft Matter Phys.* **2005**, *71*, 11701–11712.
[34] Yelamaggad, C.V.; Shashikala, I.S.; Rao, D.S.S.; Nair, G.G.; Prasad, S.K. *J. Mater. Chem*. **2006**, *16*, 4099–4102.
[35] Cui, L.; Zhao, Y.; Yavrian, A.; Galstian, T. *Macromolecules* **2003**, *36*, 8246–8252.